Algorithmic Design Method for Automated Vehicle Packaging in CAD

Runze Li[1] , Lukas Berk[2] ,

[1]BMW AG, Runze.LR.Li@bmw.de
[2]BMW AG, Lukas.Berk@bmw.de

Corresponding author: Runze Li, Runze.LR.Li@bmw.de

Abstract. Vehicle packaging design is a critical early stage in the vehicle concept development, focusing on the spatial arrangement of the driver's cockpit and passenger seating. Designing packaging that accommodates diverse driver anthropometries while satisfying ergonomic requirements and interiors accessibility remains challenging. Current approaches rely on a standard and single SAE Template as a reference driver. This template is manually positioned and iteratively revised in the vehicle packaging and supplemented by RAMSIS manikins in a later phase, but they cannot capture driver variability. The whole process is also time-consuming. This paper presents an automated method using seven digital driver models spanning a range of body sizes, generated via Algorithmic Design. Their individualized postures are obtained by solving an optimization problem subject to packaging geometry and joint angle constraints. The approach enables intuitive and dynamic assessment of vehicle packaging effectively, integrating realistic ergonomic and reachability considerations and supporting early-stage design optimization.

Keywords: Vehicle packaging design, Algorithmic Design, Digital human models, Vehicle concept
DOI: https://doi.org/10.14733/cadaps.2026.472-493

1 INTRODUCTION

1.1 Problem Statement and Motivation

In the early development phase of new vehicles, a parametric concept Computer-Aided Design (CAD) model is utilized to create a feasible concept composed of geometries. By adjusting geometric parameters, this concept is modified to accommodate project-specific objectives. One focus in the concept is the spatial allocation of the driver's workstation specified as the primary task in occupant packaging design. The allocation is aimed to accommodate different sized drivers in the common space. Drivers are supposed to reach control elements such as the steering wheel, pedals and panels and fulfill ergonomic requirements such as comfortable postures and field of view.

A standard, average, and fixed digital driver known as the SAE Template is provided by the Society of Automotive Engineers (SAE) [8, 22]. Due to the high level of simplification, the SAE Template has limited representativeness for evaluating postures of different drivers, as it cannot account for the variability in driver's anthropometry [20]. Despite the limitation, this template is commonly used in the initial packaging design for multiple purposes such as driver positioning [10, 21, 19].

Positioning of the SAE Template is a manual and iterative process based on empirical data and experiments. RAMSIS manikins are complemented in the packaging design to represent real drivers in a later phase. The posture performances of manikins are evaluated with the packaging design. If ergonomic or reachable requirements are not satisfied, the packaging design needs to be revised, and the template and manikins need to be repositioned and re-evaluated. This iterative process causes additional costs and slows down the vehicle development process.

In previous research, methods were proposed to automatically generate concepts of autonomous electric vehicles for different use cases [13, 12]. Those methods focused on autonomous vehicle concepts. In contrast to conventional vehicles, the interior design was different due to diverse customer needs in autonomous driving scenarios. For driving-oriented designs, a method was proposed to optimize vehicle packaging with SAE practices but lacked focus on drivers' postures [18]. No research had been carried out to optimize drivers' postures considering reachability and ergonomics to automate the packaging design process.

Algorithmic Design (AD) is a design approach that leverages computational algorithms to generate and manipulate 3D geometry based on specific design objectives and constraints [9, 14]. This research aims to fill the gap, proposing a novel method using AD. Seven drivers with human-like kinematics from small sizes to big sizes are generated in the vehicle's packaging. Their driving postures are optimized with a Genetic Algorithm (GA) constrained by reachable and ergonomic responses. The reachable responses are calculated between the packaging geometries and digital drivers, while the ergonomic responses are calculated from the driver's biomechanics such as joint angles. Real-world packaging designs are normally a tradeoff between reachability and ergonomics, but compromised designs could occur. To consider this aspect, weight factors are introduced to prioritize reachable or ergonomic responses to simulate different use cases. By increasing either the reachable or ergonomic weight factor, priority is given to the corresponding responses.

This method automates the positioning of digital drivers in the packaging while considering predefined reachability and ergonomics at the same time. Compared with previous methods with RAMSIS [27], this method eliminates the need for manual and iterative processes, and human-like digital drivers enables packaging evaluation from a more naturalistic way. This method allows cost reduction and higher efficiency in the current vehicle development. In addition, the application of AD bridges the code generated geometries with CAD geometries in an intuitive and interactive manner for vehicle packaging design.

1.2 Scope and Objective

Three focus points are identified in this method:

- **Compatibility**: The method should be provided as a software tool embedded within the work environment of CATIA V5. This means the method can be activated by a trigger event in CATIA, and the results of the optimization will be imported back into the current CATIA session.
- **Real-Time Feedback**: Upon the vehicle model is changed, the optimized postures should be updated in a short time.
- **Robustness**: This method should be applicable across different vehicle models.

The goal of this paper is to develop the method workflow, and present fundamental results.

1.3 Method Overview

This method comprises five steps shown in Figure 1. Algorithms in this method are developed in Python, and generated geometries are visualized in CATIA.

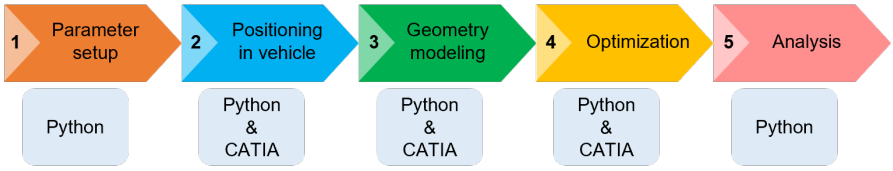

Figure 1: Method workflow.

In the first step of 'Parameter setup', parameters of reachable and ergonomic requirements, and vehicle packaging parameters are defined. This step is completed in a GUI.

To investigate driving postures, digital drivers are firstly positioned in the vehicle's cockpit. An additional digital vehicle packaging is modeled. This digital packaging can interact with digital drivers and be easily modified by the packaging parameters defined in the first step. The initial digital packaging is the remodeling of the original packaging from the vehicle architecture. In the second step, the key geometric data for remodeling is loaded from a CATIA file into Python for further execution.

In the third step, all digital drivers and the digital packaging are modeled and visualized in the vehicle architecture. By default, all drivers are initially placed at the same position within the seat adjustment area.

Next, drivers' postures are optimized with a GA constrained by predefined reachable and ergonomic responses. The geometries of optimized postures are generated and updated in the same vehicle architecture.

Lastly, optimized postures are analyzed.

2 THEORETICAL FRAMEWORK AND STATE OF THE ART

2.1 Algorithmic Design

From the perspective of design paradigms, AD is classified into textual-based and visual-based.

Textual-based AD uses computer code to generate and modify geometries directly. Figure 2 (a) shows a part of this method developed in Visual Studio Code. Textual-based AD requires basic knowledge of programming, but it can leverage external and well-developed algorithms to improve design performance. In contrast, geometries in visual-based AD are generated and modified by connecting blocks. Figure 2 (b) shows the development of the same method in Synera. Visual-based AD is more intuitive and easier to learn, but managing the blocks and parameters can be challenging when a project is complex. Additionally, users are restricted to using the integrated geometric toolboxes defined by the software, which are not as flexible as textual-based AD.

Currently, AD attracts more attention in architectural design than in vehicle concept development. However, due to its efficiency, automation, and powerful optimization capabilities, researchers use AD in the conceptual design of vehicle parts, such as a door module [5]. AD is also integrated with deep learning to design and evaluate the 3D conceptual design of wheels [29]. Additionally, AD is combined with additive manufacturing to design and produce optimized automotive components [1, 11, 30]. Despite the application of AD in the automotive industry, most applications focus on optimizing designs of vehicle parts for industrial or customized production. The application of AD in vehicle packaging design has not been investigated.

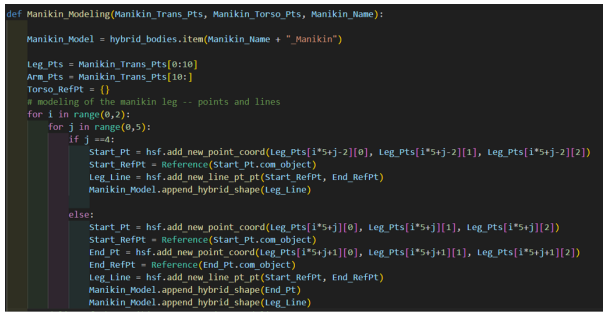

```
def Manikin_Modeling(Manikin_Trans_Pts, Manikin_Torso_Pts, Manikin_Name):

    Manikin_Model = hybrid_bodies.item(Manikin_Name + "_Manikin")

    Leg_Pts = Manikin_Trans_Pts[0:10]
    Arm_Pts = Manikin_Trans_Pts[10:]
    Torso_RefPt = []
    # modeling of the manikin leg -- points and lines
    for i in range(0,2):
        for j in range(0,5):
            if j ==4:
                Start_Pt = hsf.add_new_point_coord(Leg_Pts[i*5+j-2][0], Leg_Pts[i*5+j-2][1], Leg_Pts[i*5+j-2][2])
                Start_RefPt = Reference(Start_Pt.com_object)
                Leg_Line = hsf.add_new_line_pt_pt(Start_RefPt, End_RefPt)
                Manikin_Model.append_hybrid_shape(Leg_Line)

            else:
                Start_Pt = hsf.add_new_point_coord(Leg_Pts[i*5+j][0], Leg_Pts[i*5+j][1], Leg_Pts[i*5+j][2])
                Start_RefPt = Reference(Start_Pt.com_object)
                End_Pt = hsf.add_new_point_coord(Leg_Pts[i*5+j+1][0], Leg_Pts[i*5+j+1][1], Leg_Pts[i*5+j+1][2])
                End_RefPt = Reference(End_Pt.com_object)
                Leg_Line = hsf.add_new_line_pt_pt(Start_RefPt, End_RefPt)
                Manikin_Model.append_hybrid_shape(End_Pt)
                Manikin_Model.append_hybrid_shape(Leg_Line)
```

(a)

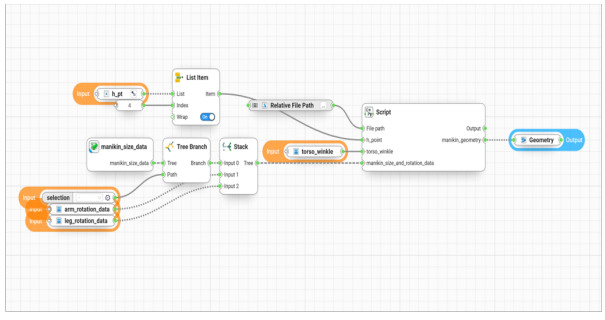

(b)

Figure 2: Design paradigms of AD: (a) textual-based and (b) visual-based.

2.2 Vehicle Packaging and Concept Development

The development of a new vehicle concept often begins with a predecessor vehicle. However, it is challenging to use previous concepts, as previous geometries are constrained by old technologies and functions. Therefore, new geometric requirements should be considered in the new vehicle concept design. To address this issue, a brand-new vehicle concept could be designed, but this process is time-consuming for both design and validation, resulting in low efficiency. Alternatively, an updated vehicle concept can be obtained by optimizing the previous vehicle concept with new geometric boundaries.

A method was proposed to optimize an existing Battery Electric Vehicle (BEV) concept to plan packaging for autonomous vehicles [13]. In another research, the influence of autonomous driving on the vehicle concept design was evaluated [12]. Additionally, two studies introduced a method to identify customer-relevant properties for autonomous vehicle concepts [24, 25]. The research mainly focused on autonomous vehicle concepts since autonomous driving was a revolutionary technology introduced for concept designs. For the generation and optimization of conventional vehicle concepts, public research is limited. One research focused on simultaneous placement of the seat and steering wheel adjustment areas to optimize vehicle packaging [18].

3 Methodology

3.1 MODELING OF DIGITAL DRIVERS

3.1.1 Skeleton

Digital drivers are modeled with skeletons, where points represent body joints and lines represent body segments. When holding the steering wheel, a driver's hands are assumed to be closed-fist shapes. The MCP

(metacarpophalangeal) points of the middle fingers are modeled as hand-effect points to reach the steering wheel. The length of the driver's lower arm is the distance between the hand-effect point and the elbow point. Wrist points are assumed to be fixed on the lower arm lines and are not modeled. Figure 3 shows the digital driver skeleton.

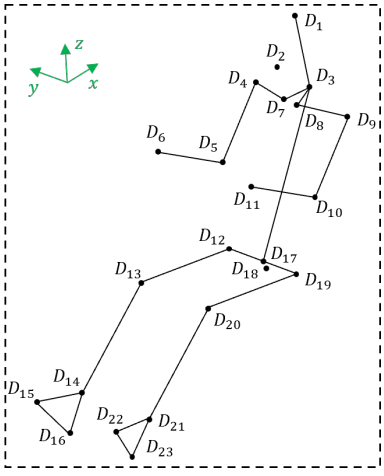

Figure 3: Digital driver skeleton. D_1: head vertex, D_2: mid-eye point, D_3: chest, D_4: right shoulder, D_5: right elbow, D_6: right-hand effect point, D_7: right clavicle, D_8: left clavicle, D_9: left shoulder, D_{10}: left elbow, D_{11}: left-hand effect point, D_{12}: right hip, D_{13}: right knee, D_{14}: right ankle, D_{15}: right ball of foot, D_{16}: right heel, D_{17}: hip-center point, D_{18}: H point, D_19: left hip, D_{20}: left knee, D_{21}: left ankle, D_{22}: left ball of foot, D_{23}: left heel.

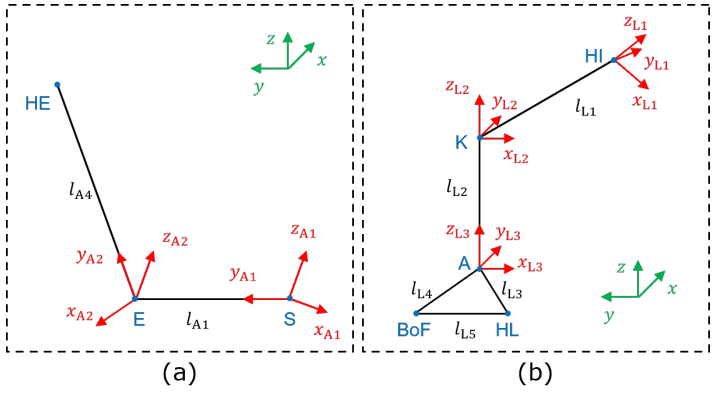

Figure 4: Kinematics of the digital driver's: (a) right arm and (b) right leg.

3.1.2 Kinematics

The digital driver is modeled with kinematics in the arms, legs, and upper body to replicate movement of human drivers. The movements are simplified as 3D rotations around joint points. Figure 4 shows a sketch of the rotational kinematics of the right arm and leg, where S, E, HE, HI, K, A, HL, and BoF represent points

of the shoulder, elbow, hand effect, hip, knee, ankle, heel, and ball of foot. Mirror effects are not considered, so left and right arms and legs share the same kinematics.

As illustrated in Figure 4, one arm has two rotatable joints: one at S and another at the E. Similarly, one leg has three rotatable joints: one at HI, one at K, and one at A. The rotations at joint points are independent from each other, and each rotatable joint has three degrees of freedom (DoF), corresponding to rotations around the local joint's x, y, and z axes.

Practically, several joint points have restricted DoFs. For example, the elbow point has one DoF, so that the lower arm line l_{A4} can only rotate about the z_{A2} axis at the E point. DoFs of the driver's arm and leg are summarized in Table 1. In the subscript, 'S', 'E', 'HI', 'K' and 'A' specifies the joint points. 'L' and 'R' represent the 'left' or 'right' side of the point. 'x', 'y' and 'z' in the superscript represents the rotating axis at the joint point. For instance, x^{x}_{SL} indicates the rotational degrees of the left upper arm about the x-axis at the left shoulder point. In addition to arms and legs, the upper body can also rotate about the local y axis at the hip center point D_{17}, representing the forward or backward movement of the upper body.

Joint point	*Rotation about the local axis (Unit: degree)*		
	x axis	*y axis*	*z axis*
S	x^{x}_{SL}; x^{x}_{SR}	x^{y}_{SL}; x^{y}_{SR}	x^{z}_{SL}; x^{z}_{SR}
E	None	None	x^{z}_{EL}; x^{z}_{ER}
HI	x^{x}_{HIL}; x^{x}_{HIR}	x^{y}_{HIL}; x^{y}_{HIR}	x^{z}_{HIL}; x^{z}_{HIR}
K	None	x^{y}_{KL}; x^{y}_{KR}	None
A	x^{x}_{AL}; x^{x}_{AR}	x^{y}_{AL}; x^{y}_{AR}	x^{z}_{AL}; x^{z}_{AR}

Table 1: Modelled DoFs in the digital driver's arm and leg.

The coordinate transformation is applied to solve the rotation kinematics and obtain global coordinates of joint points. In 3D space, the composite rotation matrix is given as follows:

$$\mathbf{R}_{zyx}(\phi,\theta,\psi)=\mathbf{R}_{z}(\phi)\mathbf{R}_{y}(\theta)\mathbf{R}_{x}(\psi) \tag{1}$$

with separated rotation matrices as:

$$\mathbf{R}_{z}(\phi)=\begin{bmatrix}\cos\phi & -\sin\phi & 0\\ \sin\phi & \cos\phi & 0\\ 0 & 0 & 1\end{bmatrix},\mathbf{R}_{x}(\psi)=\begin{bmatrix}1 & 0 & 0\\ 0 & \cos\psi & -\sin\psi\\ 0 & \sin\psi & \cos\psi\end{bmatrix},\mathbf{R}_{y}(\theta)=\begin{bmatrix}\cos\theta & 0 & \sin\theta\\ 0 & 1 & 0\\ -\sin\theta & 0 & \cos\theta\end{bmatrix}$$

Take the right arm in Figure 4 as an example. The initial coordinate of E in the local $x_{\mathrm{A1}}y_{\mathrm{A1}}z_{\mathrm{A1}}$ coordinate system of S is defined as $\mathbf{p}^{\mathrm{A1}}_{\mathrm{E}}=\begin{bmatrix}0 & l_{\mathrm{A1}} & 0\end{bmatrix}^{\mathrm{T}}$. The rotation matrix at S is $\mathbf{R}_{\mathrm{A1}}=\mathbf{R}_{z}(x^{z}_{\mathrm{SR}})\mathbf{R}_{y}(x^{y}_{\mathrm{SR}})\mathbf{R}_{x}(x^{x}_{\mathrm{SR}})$. The global coordinate of E is calculated as:

$$\mathbf{p}_{\mathrm{E}}=\mathbf{R}_{\mathrm{A1}}\cdot\mathbf{p}^{\mathrm{A1}}_{\mathrm{E}} \tag{2}$$

For HE, coordinate transformation is applied two times due to two individual rotations at S and E. The initial coordinate of HE in the local $x_{\mathrm{A2}}y_{\mathrm{A2}}z_{\mathrm{A2}}$ coordinate system of E is defined as $\mathbf{p}^{\mathrm{A2}}_{\mathrm{HE}}=\begin{bmatrix}0 & l_{\mathrm{A4}} & 0\end{bmatrix}^{\mathrm{T}}$. The corresponding rotation matrix is defined as $\mathbf{R}_{\mathrm{A2}}=\mathbf{R}_{z}(x^{z}_{\mathrm{ER}})\mathbf{R}_{y}(0)\mathbf{R}_{x}(0)$. Following the rotation at S above, the global coordinate of HE is obtained as:

$$\mathbf{p}_{\mathrm{HE}}^{\mathrm{A1}} = \mathbf{p}_{\mathrm{E}}^{\mathrm{A1}} + \mathbf{R}_{\mathrm{A2}} \cdot \mathbf{p}_{\mathrm{HE}}^{\mathrm{A2}} \tag{3}$$

Solving the kinematics of legs is in a similar manner to the arms. The driver's torso points are directly modeled in the global coordinate. By synthesizing the torso points with the transformed arm and leg points, the driver's skeleton is modeled in the global coordinate.

3.1.3 Driver Models

Driver sizes are typically represented by the 5th percentile female, 50th percentile male, and 95th percentile male. Body height is often regarded as the primary anthropometric distinguishing feature among people. However, it is observed that the proportion of leg length and trunk length can vary for a certain body height. This phenomenon is known as the seated giant (long trunk, short legs) and seated dwarf (short trunk, long legs) shown in Figure 5 [6, p. 183].

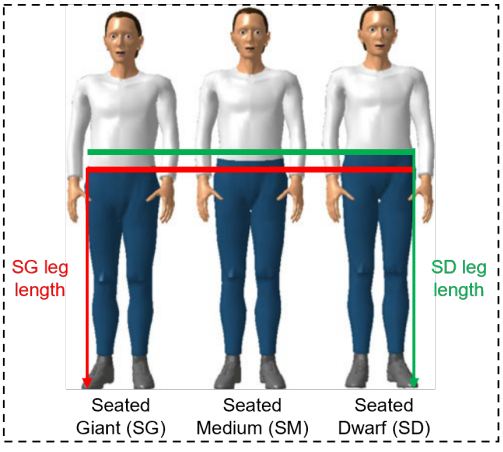

Figure 5: Representation of the variation in leg length and trunk length for the same body height for Seated Giant, normally proportioned person and Seated Dwarf.

In this method, body proportion is applied to drivers with small and big body sizes. Specifically, SG, SM and SD drivers are modeled for the 5th percentile female and the 95th percentile male. One SD driver is modeled for the 50th percentile male. In summary, seven digital drivers are modelled and labeled as 05FSG, 05FSM, 05FSD, 50MSD, 95MSG, 95MSM, and 95MSD, representing the driver group, gender, and body proportions (Figure 6). RAMSIS data is used to model these digital drivers.

3.2 MODELING OF DRIVING RESPONSES

Driving requirements are modeled as responses of an optimization problem for digital drivers to carry out driving tasks. These requirements include the driver's reachability and ergonomics. The ergonomic responses are classified into two categories: vehicle-constrained responses and individual biomechanical constrained responses.

3.2.1 Digital Vehicle Packaging

A simplified digital packaging is modeled in this section. The geometries in the digital packaging can be modified via packaging parameters defined by users, enabling different designs in the same vehicle architecture.

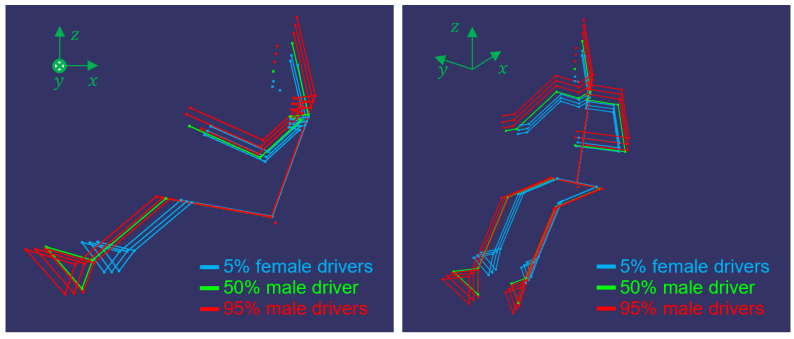

Figure 6: Digital driver models with seven different anthropometric definitions: (a) from left view and (b) from front left view.

The initial digital packaging is modeled with geometric data of the vehicle's original packaging design. As shown in Figure 7 in a SUV architecture model, the digital packaging is composed of the steering area, pedal area, seat adjustment area and three single points (V_1, V_2 and V_3). The digital packaging and vehicle architecture are both modeled in the global coordinate system.

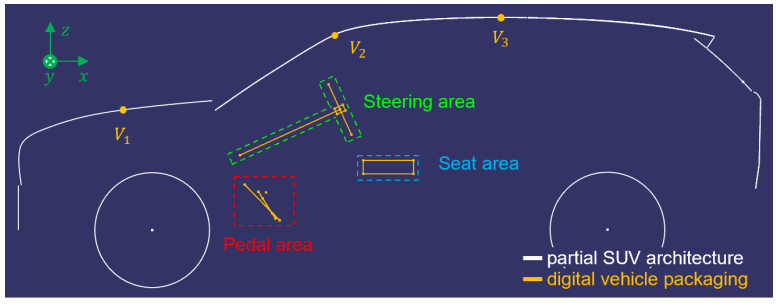

Figure 7: A SUV architecture model with a simplified digital packaging in the concept phase.

Modeling of the steering wheel is visualized in Figure 8 (a). The position of the steering wheel is adjusted by changing the length of the steering axis x_{STL} and the angle of the steering axis x_{STA}. The center point of the steering wheel V_8 forms the steering adjustment area $ST_1ST_2ST_3ST_4$. The points V_4,V_5,V_6 and V_7 are respectively the top, leftmost, bottom and rightmost points of the steering wheel. The steering wheel can be adjusted in the adjustment area.

From 8 (b), the area $V_{10}V_{11}V_{12}V_{13}$ is the left footrest pedal, where the digital driver puts the left foot. Points V_{14} and V_{20} are respective effect points on the brake pedal and gas pedal. The driver's right ball of foot point should approach either one point to step on either the brake or gas pedal. $V_{15}V_{16}V_{17}V_{18}V_{19}$ indicates the modeled gas pedal. The bottom points V_{11} and V_{12} are assumed to be on the vehicle's floor. The driver's left and right heel points are supposed to have the same global z coordinate as V_{11} or V_{12}.

The driver's view lines and the seat area are shown in Figure 9. Both view lines start from the driver's mid-eye point D_2. The downward view line is tangent to the engine hood at V_1. This tangent point is assumed to be fixed for all digital drivers. V_2 is the highest point of the windshield, and the upward view line is the boundary view line that the driver can look upward. The downward and upward view lines form the driver's maximum visual angle looking through the window shield.

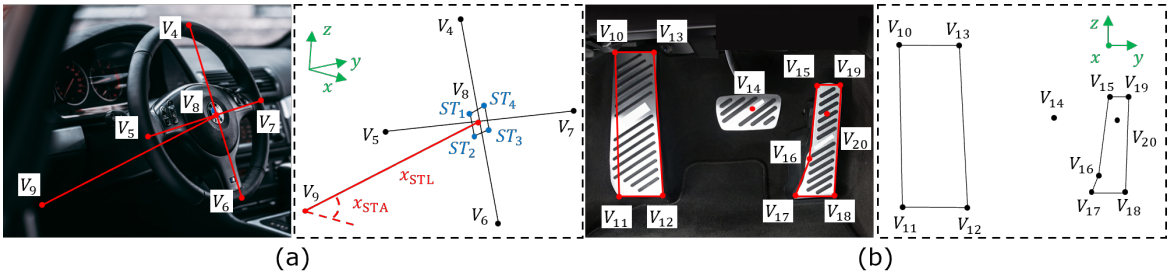

Figure 8: Modeling of: (a) the steering wheel area and (b) the pedal area.

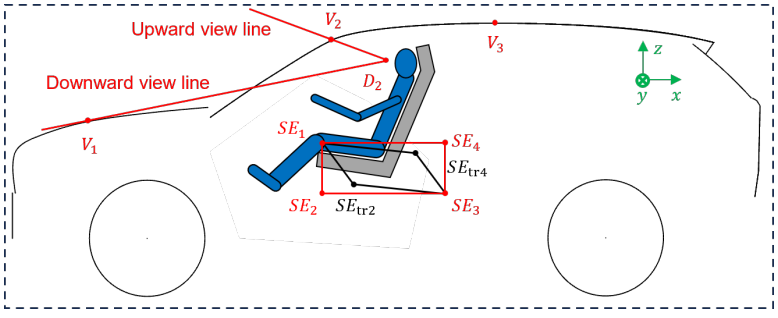

Figure 9: Modeling of view lines and the seat area.

The area $SE_{\text{tr1}}SE_{\text{tr2}}SE_{\text{tr3}}SE_{\text{tr4}}$ refers to the true seat adjustment area. While driving a vehicle, the position of the driver's H-point varies in the true seat adjustment area by moving the seat forward or backward and upward or downward. In the digital packaging, the seat adjustment area is simplified as a rectangle area as $SE_1SE_2SE_3SE_4$ based on the true seat adjustment area. The left top point SE_1 is overlapped with SE_{tr1}, and the right bottom point SE_3 is overlapped with SE_{tr3}.

V_3 is the highest roof point and indicates the freedom of the driver above head.

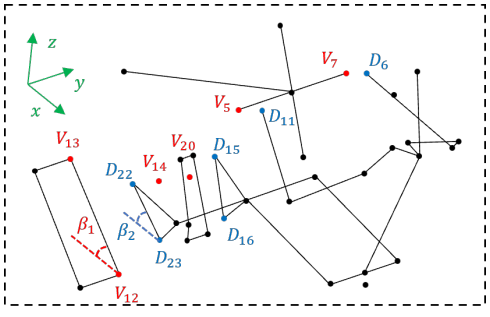

Figure 10: Modeling of reachable responses of hands and feet.

3.2.2 Reachable Responses

Reachable responses outline fundamental driving tasks illustrated in Figure 10: (1) the driver's left and right hands are holding the steering wheel, (2) the driver's left foot is placed on the footrest pedal, (3) the driver's

right foot steps on the gas or the brake pedal, and (4) the driver's left and right heels are placed on the floor.

Reachable responses are modeled as angular differences indicated by 'diff' and differences of Euclidean distance indicated by 'dist' summarized in Table 2. When res_1 and res_2 equal zero, the driver is assumed to be holding the steering wheel firmly. When res_3 and res_4 equal zero, the driver's left foot is placed on the left footrest pedal with the left heel point placed on the pedal's right bottom point. When res_5 and res_6 equal zero, the driver's right foot is stepping on either the brake or gas pedal, and the right heel point is placed on the floor.

Response	*Definition*	*Description*
res_1	$\mathrm{dist}(D_{11}, V_5)$	Distance between the left HE and the leftmost point of the steering wheel.
res_2	$\mathrm{dist}(D_6, V_7)$	Distance between the right HE point and the rightmost point of the steering wheel.
res_3	$\mathrm{dist}(D_{23}, V_{12})$	Distance between the left HL and the right bottom point of footrest pedal.
res_4	$\mathrm{diff}(\beta_1, \beta_2)$	Difference between the footrest pedal and the bottom line of left foot in the global xz plane.
res_5	$\mathrm{dist}(D_{15}, V_{14})$ or $\mathrm{dist}(D_{15}, V_{20})$	Distance between the right BoF and the effect point of brake pedal or gas pedal.
res_6	$\mathrm{dist}(z(D_{16}), z(V_5))$	Distance of the right HL and the right bottom point of footrest in global z axis.

Table 2: Reachable responses.

3.2.3 Ergonomic Responses

Static ergonomics is considered in this method. Vehicle-constrained responses refer to the ergonomic interactions between the driver and the packaging shown in Figure 11. They include head freedom, view angles, leg freedom, and knee freedom.

Head freedom, denoted as $d_{\mathrm{H}} = \mathrm{dist}(z(D_1), z(V_3))$, measures the height difference between the driver's head vertex D_1 and the highest roof point V_3. A threshold value, T_{headroom}, is defined as the minimum head freedom that should be maintained.

View angles are defined by included angles between either the downward view line or the upward view line and a horizontal line. α_1 is the downward view angle and α_2 is the upward view angle. Correspondingly, T_{down} and T_{up}, are the minimum values that view angles should achieve.

Leg and knee freedom refers to the available space between the steering wheel and the driver's legs and knees. The left leg freedom d_{LL} and right leg freedom d_{LR} represent respectively the distance between the steering wheel's bottom point V_6 and the driver's left leg line $D_{19}D_{20}$ and the driver's right leg line $D_{12}D_{13}$. The left knee freedom d_{KL} and the right knee freedom d_{KR} represent respectively the distance between the steering axis V_8V_9 and the driver's left knee point D_{20} or right knee point D_{13}. Threshold values T_{legroom} and T_{kneeroom} are respectively the minimum leg and knee freedom.

Individual biomechanical constrained responses are modeled from the driver's joint angles in angular differences.These responses evaluate the driver's comfort in a driving posture. λ_{torso} is the torso angle between the driver's central torso line D_3D_{17} and a vertical line. λ_{S} is the shoulder angle between the driver's upper arm and central torso line. The elbow angle between the upper arm and lower arm is indicated as λ_{E}. The

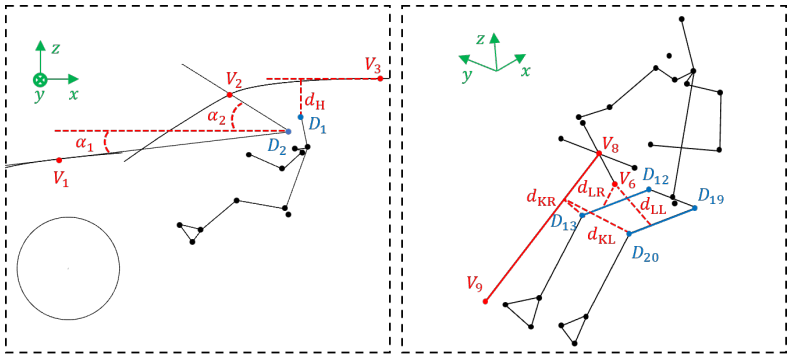

Figure 11: Modeling of vehicle-related ergonomic responses: (a) the view angles and head freedom and (b) the leg freedom and knee freedom.

hip angle λ_{HI} is the angle between the upper leg and the central torso line. λ_{K} is the knee angle between the upper leg and lower leg. The ankle angle λ_{A} is the angle between the lower leg and the upper foot line. In addition to the torso angle, other joint angles have the left and right cases indicated by 'L' and 'R'. For example, λ_{SL} and λ_{SR} are respectively the left and right shoulder angles. Figure 12 shows the joint angles. An ergonomic posture is predefined by given reference values from λ_1 to λ_6. When every joint angle is equal to the respective reference value, the driving posture is considered as fully ergonomic.

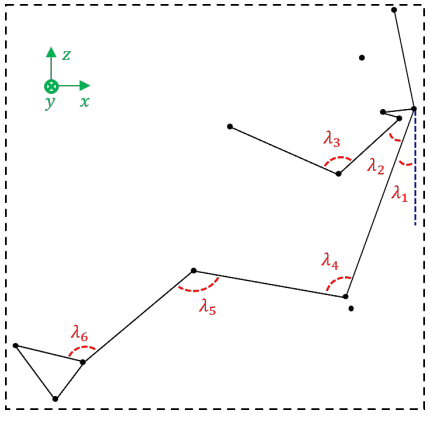

Figure 12: Joint angles for ergonomic evaluation.

Overall ergonomic responses are summarized in Table 3.

3.3 Optimization Problem Formulation and Results Evaluation

The optimization problem is formulated by minimizing the reachable and ergonomic responses, and Each driver's posture is optimized individually.

The tradeoff between reachability and ergonomics is considered for different design objectives. To prioritize reachable and ergonomic responses, the Reachable Weight Factor (RWF) and the Ergonomic Weight Factor (EWF) are introduced. These coefficients were used to multiply corresponding responses. By increasing either

Response	*Definition*	*Description*
res_7	0	$d_{\mathrm{H}} \geq T_{\mathbf{headroom}}$.
	$T_{\mathbf{headroom}} - d_{\mathrm{H}}$	$d_{\mathrm{H}} < T_{\mathbf{headroom}}$.
res_8	0	$\alpha_1 \geq T_{\mathbf{down}}$.
	$T_{\mathbf{down}} - \alpha_1$	$\alpha_1 < T_{\mathbf{down}}$.
res_9	0	$\alpha_2 \geq T_{\mathbf{up}}$.
	$T_{\mathbf{up}} - \alpha_2$	$\alpha_2 < T_{\mathbf{up}}$.
res_{10}	0	$d_{\mathrm{LL}} \geq T_{\mathbf{legroom}}$.
	$T_{\mathbf{legroom}} - d_{\mathrm{LL}}$	$d_{\mathrm{LL}} < T_{\mathbf{legroom}}$.
res_{11}	0	$d_{\mathrm{LR}} \geq T_{\mathbf{legroom}}$.
	$T_{\mathbf{legroom}} - d_{\mathrm{LR}}$	$d_{\mathrm{LR}} < T_{\mathbf{legroom}}$.
res_{12}	0	$d_{\mathrm{KL}} \geq T_{\mathbf{kneeroom}}$.
	$T_{\mathbf{knwwroom}} - d_{\mathrm{KL}}$	$d_{\mathrm{KL}} < T_{\mathbf{kneeroom}}$.
res_{13}	0	$d_{\mathrm{KR}} \geq T_{\mathbf{kneeroom}}$.
	$T_{\mathbf{knwwroom}} - d_{\mathrm{KR}}$	$d_{\mathrm{KR}} < T_{\mathbf{kneeroom}}$.
res_{14}	$\lambda_{\mathrm{torso}} - \lambda_1$	Difference between torso angle and λ_1.
res_{15}	$\lambda_{\mathrm{SL}} - \lambda_2$	Difference between left shoulder angle and λ_2.
res_{16}	$\lambda_{\mathrm{SR}} - \lambda_2$	Difference between right shoulder angle and λ_2.
res_{17}	$\lambda_{\mathrm{EL}} - \lambda_3$	Difference between left elbow angle and λ_3.
res_{18}	$\lambda_{\mathrm{ER}} - \lambda_3$	Difference between right elbow angle and λ_3.
res_{19}	$\lambda_{\mathrm{HIL}} - \lambda_4$	Difference between left hip angle and λ_4.
res_{20}	$\lambda_{\mathrm{HIR}} - \lambda_4$	Difference between right hip angle and λ_4.
res_{21}	$\lambda_{\mathrm{KL}} - \lambda_5$	Difference between left knee angle and λ_5.
res_{22}	$\lambda_{\mathrm{KR}} - \lambda_5$	Difference between right knee angle and λ_5.
res_{23}	$\lambda_{\mathrm{AL}} - \lambda_6$	Difference between left ankle angle and λ_6.
res_{24}	$\lambda_{\mathrm{AR}} - \lambda_6$	Difference between right ankle angle and λ_6.

Table 3: Overall ergonomic responses.

RWF or EWF, the reachable performance or ergonomic performance tends to be more satisfied. The weighted responses are obtained as follows:

$$\begin{aligned} wres_i &= res_i \times RWF, \quad 1 \le i \le 6, \\ wres_i &= res_i \times EWF, \quad 7 \le i \le 24. \end{aligned} \tag{4}$$

Genetic Algorithm (GA) shows advantages in solving nonlinear problems [3], so the weighted responses controlled by RWF and EWF are minimized by a GA in this study. Independent variables are variables in Table 1 and the torso angle, and the objective function is formulated as:

$$\underset{x}{\text{minimize}} \qquad f(x) = \sum_{i=1}^{24} wres_i^2. \tag{5}$$

The original reachable and ergonomic responses are used for evaluation, because they describe the drivers' real optimized postures. The postures were evaluated from the perspectives of reachability, ergonomics, and overall performances. The responses are normalized to mitigate the influence of distance and angular differences:

$$y = \frac{x}{\sigma + x}, \quad 0 \le x \le +\infty, \tag{6}$$

where σ is the normalization parameter and controls the scaling.

The reachable score of an optimized seating posture is obtained by:

$$score_{\mathrm{R}} = 100 \times \left(1 - \frac{res_{\mathrm{R}}}{\sigma_{\mathrm{R}} + res_{\mathrm{R}}}\right), \quad res_{\mathrm{R}} = \frac{\sum_{i=1}^{6} |res_i|}{6}. \tag{7}$$

The ergonomic score is obtained by:

$$score_{\mathrm{E}} = 100 \times \left(1 - \frac{res_{\mathrm{E}}}{\sigma_{\mathrm{E}} + res_{\mathrm{E}}}\right), \quad res_{\mathrm{E}} = \frac{\sum_{i=7}^{24} |res_i|}{18}. \tag{8}$$

The overall performance incorporates both reachable and ergonomic responses and shows a comprehensive assessment of the posture. The overall score is calculated as:

$$score_{\mathrm{O}} = 100 \times \left(1 - \frac{res_{\mathrm{O}}}{\sigma_{\mathrm{O}} + res_{\mathrm{O}}}\right), \quad res_{\mathrm{O}} = \frac{\sum_{i=1}^{24} |res_i|}{24}. \tag{9}$$

4 RESULTS AND DISCUSSIONS

The Integrated Development Environment (IDE) of Python (Version: 3.11.2) is Visual Studio Code (Version: 1.106.3). The software for vehicle geometry design is CATIA V5. A Python package pyCATIA 0.9.2 is applied to visualize the Python generated geometries in an active .part session in CATIA. Other packages used are NumPy and ypstruct. The computer is equipped with an Intel Core i7 2.1 GHz Computer Processing Unit (CPU) and 32 GB random-access memory (RAM).

Threshold values in the vehicle-related ergonomic responses vary across different vehicle architecture models. This method is developed on a SUV architecture, and the reference threshold values are assumed by the author to ensure good visibility and comfort in Table 4.

Ranges of human joint angles for ergonomic driving postures are summarized from different sources [28]. Reference values of joint angles for an ergonomic posture taken for this paper are shown in Table 5.

A standard GA is the optimizer. Parents are selected with roulette wheel selection and applied uniform crossover. In mutation process, genes are added random values controlled by step size under mutation rate.

Threshold	*Value*	*Unit*
T_{headroom}	80	mm
T_{up}	7	°(degrees)
T_{down}	7	°(degrees)
T_{legroom}	90	mm
T_{kneeroom}	200	mm

Table 4: Reference threshold values for vehicle-related ergonomic responses.

Joint	*Value*
λ_1	26.9 °
λ_2	22.1 °
λ_3	125.5 °
λ_4	99.3 °
λ_5	116.9 °
λ_6	136.6 °

Table 5: Benchmark joint angles for an ergonomic seating posture.

Fitness is computed with the loss function. The parameters are listed in Table 6. The max. iterations, population size and children size are selected large values to obtain global optimal as much as possible and ensure robustness of this method across different architecture models. The computational load is not discussed.

Parameter	*Value*
Max. iterations	500
Population size	400
Children size	400
Selection probability para.	1
Crossover rate	0.6
Mutation rate	0.15
Mutation step size	0.8

Table 6: GA parameters.

4.1 Seating Postures Optimization

Drivers' postures are optimized in a SUV architecture model. RWF and EWF equals one, and reachable and ergonomic responses share the same weight during optimization. As shown in Figure 13, 5th percentile females are seated more forward compared to the 95th percentile males, which aligns with empirical observations. From score evaluation, male drivers have better reachable performances compared to female drivers, while all of them

have similar ergonomic scores around 60. Thus, male drivers have higher overall scores than females. Among male drivers, 50MSG, 95MSG, and 95MSM have better reachable scores than 95MSD does. In contrast, female drivers have similar reachable, ergonomic and overall scores. It can be concluded that the current packaging design should pay attention to the reachability of females and 95MSD and ergonomics of all drivers to have better posture performances.

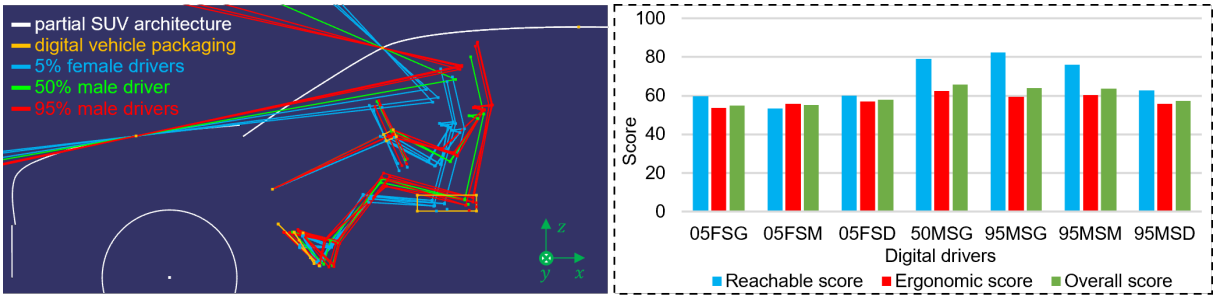

(a) (b)

Figure 13: Posture optimization in a SUV architecture with RWF=1 and EWF=1: (a) the optimized postures and (b) results evaluation.

The distribution of drivers' steering wheel center points (CPs) and H points (HPs) is critical for packaging design. The CPs and HPs from Figure 13 are detailed in Figure 14. All drivers tend to position the steering wheel in the upper half of the steering adjustment area. Female drivers prefer a short length of the steering wheel, while male drivers prefer a longer one. For HPs, all drivers are seated in the lower half of the seat adjustment area. Male HPs are clustered near the right bottom corner, which is similar to real-world epirical results [15]. HPs of 5th female drivers are positioned in the middle area, while they are mostly positioned near the left upper corner from practical experience [26, p. 39] [2, p. 273] . From the distributions of CPs and HPs, a new steering wheel adjustment area and seat adjustment area are proposed to improve posture performance. The results are detailed in the next section.

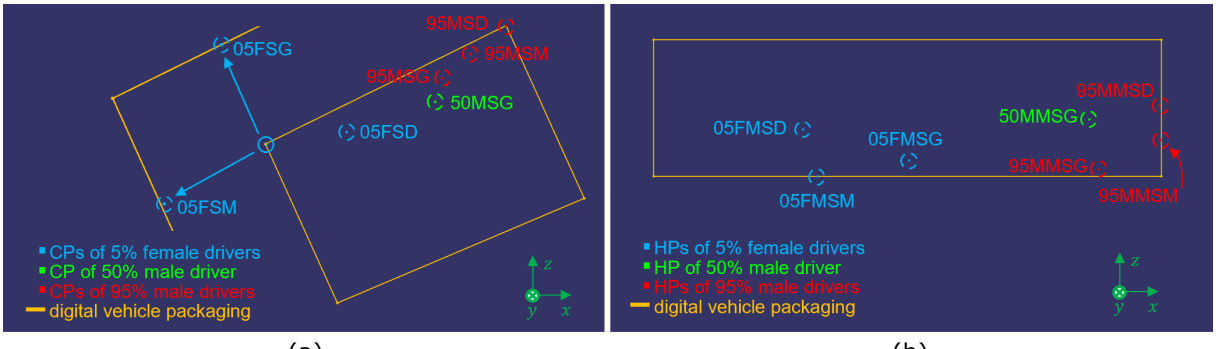

(a) (b)

Figure 14: Distribution of drivers' CPs and HPs in the optimized postures in SUV: (a) CPs and (b) HPs.

The average scores of all seven drivers' optimized postures with increasing RWF and EWF are shown in Figure 15. When RWF increases and EWF=1, the average reachable score rises and stabilizes at around 85 when RWF=4. At the same time, the ergonomic score decreases, and the overall score remains unchanged in

the beginning and decreases later. In comparison, the average ergonomic score increases and stays at around 90 when EWF=5.5 as EWF increases and RWF=1. The reachable score decreases, while the overall score initially increases and then decreases.

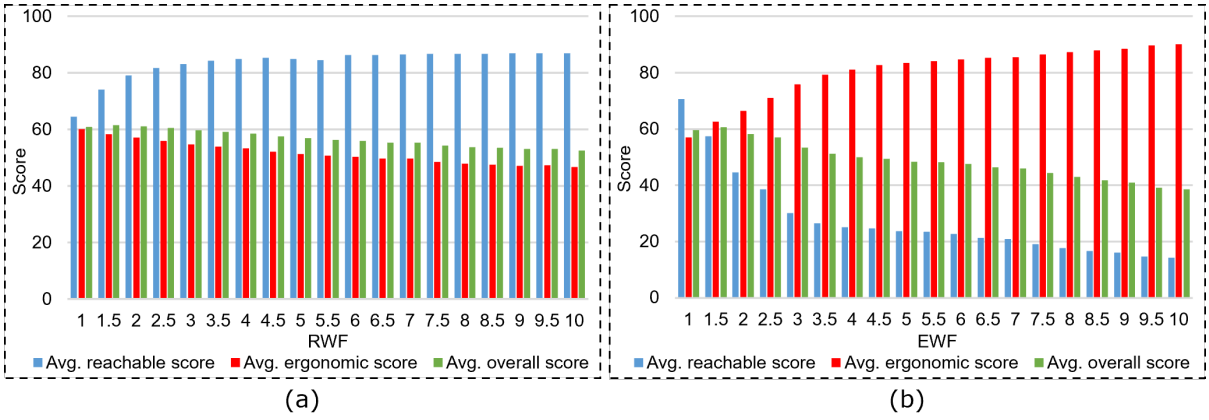

Figure 15: Average scores of all drivers' postures with varying weight factors: (a) RWF and (b) EWF.

It is observed from the comparative results of RWF and EWF that the optimized postures are balanced results between reachable and ergonomic responses when RWF and EWF are equal. Increasing either weight factor has a negative effect on the other responses. The reachable and ergonomic responses are contradictory aspects for the optimized postures in the current packaging design. A new packaging design is required to improve both reachability and ergonomics. In addition, the influence of ergonomic responses on reachable responses is greater than the reverse. Ergonomic responses also influence the overall score more than reachable responses. The new packaging designs should address more ergonomic responses if the overall score is aimed to be improved.

Figure 16 shows the optimized postures under two extreme scenarios with RWF=10, EWF=1 and RWF=1, EWF=10. All postures are upright and unergonomic when RWF equals ten and EWF equals one. On the other hand, drivers have problems reaching the steering wheel and pedals properly when EWF is much larger than RWF. Besides, female drivers are seated higher with a large EWF compared to postures in Figure 13. The positions of their HPs are closer to empirical results. However, females are still seated in the middle instead of the front area to reduce violation of reachable requirements.

The predefined ergonomic posture could be one reason for the unbalanced influence of EWF and RWF. When RWF is large and reachable constraints are fulfilled, all drivers' postures are close to the benchmark posture, and the ergonomic score does not decrease much. Conversely, the reachability is not satisfactory when the benchmark ergonomic posture is achieved with a large EWF.

4.2 Iterative Design of Occupant Packaging

New packaging designs are modeled in the vehicle architecture via modifying packaging parameters. Drivers' postures are optimized in the new design and analyzed. From optimization results, another new packaging can be proposed. Through iterations of new designs and posture optimization, it could be possible to find a packaging design that achieves better posture performance for all drivers in the design space of vehicle architecture.

From Figure 14, a new packaging design can be proposed based on the distribution of CPs and HPs. The steering wheel adjustment area is shifted upward with a larger range to adjust the steering axis length, while

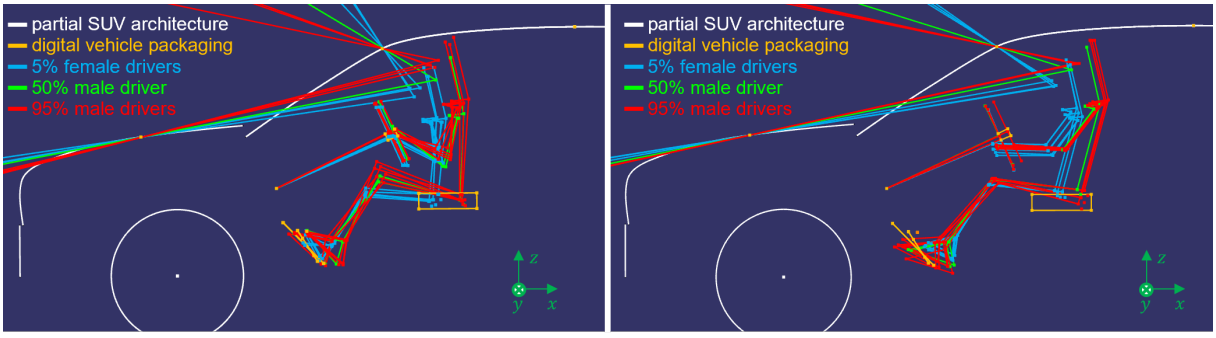

Figure 16: Posture optimization with extreme weight factors: (a) RWF=10 and EWF=1 and (b) RWF=1 and EWF=10.

the seat adjustment area is shifted downward and backward. The two new areas and CPs and HPs of the respective optimized postures are shown in Figure 17. Compared with the previous design, drivers' CPs are all positioned in the middle and lower part of the steering adjustment area. Female drivers prefer a short steering axis length, while the 95% male drivers have longer lengths and 50MSG has a middle one. Male drivers' HPs are positioned around the top right corner, and female drivers' HPs are positioned in the center.

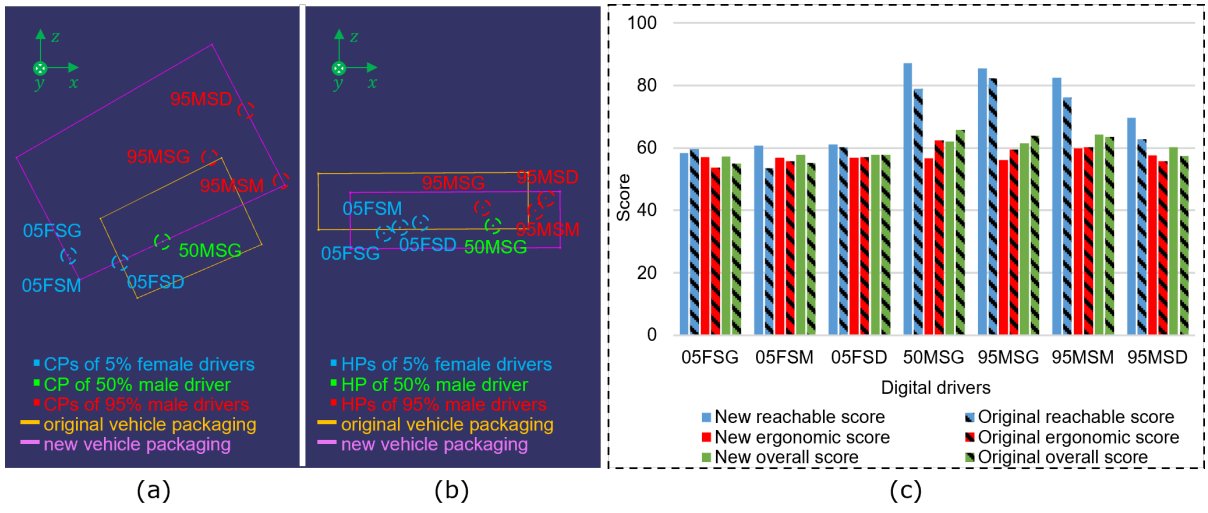

Figure 17: Posture optimization in a new packaging design in SUV with RWF=1 and EWF=1: (a) the distribution of CPs, (b) the distribution of HPs and (c) comparative evaluation.

Comparative evaluations of optimized postures in the new and previous packaging are presented in the right figure. Male drivers have higher reachable scores. The ergonomic performance of 50MSG and 95MSG decreases and that of 95MSD increases. The ergonomic performance of 95MSM remains similar. There is a decrease in overall scores of 50MSM and 95MSG, and an increase in overall scores of 95MSM and 95MSD. For female drivers, 05FSG has a worse reachable but improved ergonomic performance, but the overall performance improves. For 05FSM, the reachable, ergonomic, and overall performances are improved.

For 05FSD, the reachable performance improves slightly, and the ergonomic and overall performance remains unchanged.

4.3 Universality and Flexibility in Extension

Geometric data of the digital packaging is loaded from the vehicle architecture in a CAD file in this method. Changing the vehicle architecture, the geometric data updates respectively. The SUV architecture is switched to a sedan architecture to show the universality of this method. With RWF = 1 and EWF = 1, drivers' postures are optimized and analyzed in the original packaging of a sedan architecture model. The model can also be switched to sports architecture or others.

Compared to the optimized postures in SUV, postures in the sedan have a lower position shown in Figure 18. Similarly, female drivers are seated in the front part of the seat adjustment area, while male drivers are positioned in the right bottom corner. From score evaluation, this sedan's packaging design offers better reachability for 50MSG, 95MSG, and 95MSM, and their respective scores are over 70. Female drivers' reachable performances are around 60 and inferior to the above-mentioned drivers. 95MSD has the worst reachable score, which is around 50. This packaging design offers similar ergonomic performances to all drivers, and their ergonomic scores are between 50 and 60. To improve the packaging design in this sedan, the reachability of female drivers and 95MSD should be addressed. In addition, better ergonomic performance of all drivers should be considered.

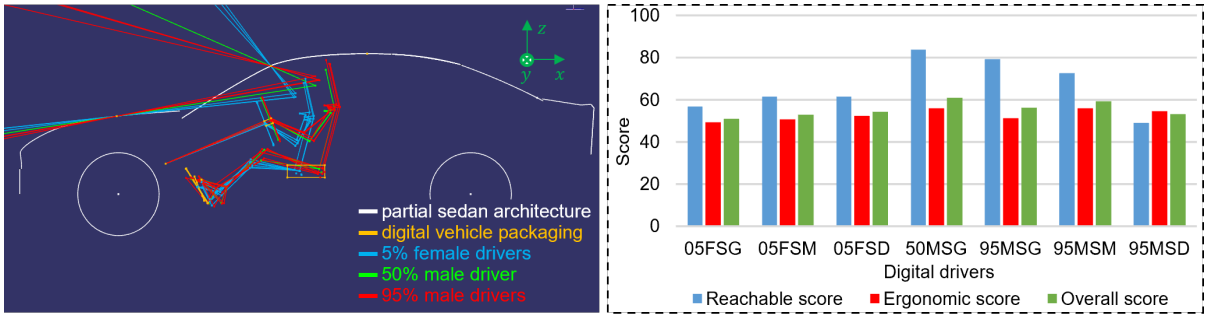

(a) (b)

Figure 18: Posture optimization in a sedan architecture with RWF=1 and EWF=1: (a) the optimized postures and (b) results evaluation.

While the digital packaging design is simplified in this paper, this method has flexibility to include more geometric constraints simply. The vehicle architecture in a CAD file has complete geometric information of the vehicle. When the geometric data of the simplified digital packaging is loaded, geometric data of other packaging parts such as the dashboard, touchscreen and armrest can simultaneously be loaded. Based on the loaded data, geometry of packaging parts is modeled. The respective weighted responses of the newly modeled geometry are added into the loss function for optimization. In this way, the new geometry is included in the boundary conditions as constraints. For example, a visual angle can be modeled from visual lines connecting the driver's mid-eye point and dashboard geometry. This response evaluates the driver's visibility on the dashboard. The requirement of the driver's dashboard visibility is considered while solving the optimization problem.

4.4 Discussion and Limitation

The optimized postures of male drivers in the SUV and sedan are consistent with empirical observations. However, the HP distributions of 5th percentile female drivers deviate from empirical findings. One possible explanation is the use of the simplified digital vehicle packaging. In one research, female drivers were found generally less well accommodated in vehicles compared to large male drivers [23]. The simplified packaging does not capture the full range of geometries in a real vehicle, thereby diminishing the geometric effects that influence posture optimization for female drivers. Another potential factor is the use of the modeled ergonomic responses that do not account for gender-specific differences. Previous research [7] has shown that male drivers typically maintained a greater distance from the steering wheel, whereas female drivers tend to sit closer. Female drivers also tend to adopt a more upright and higher seating position than male drivers. Applying identical ergonomic responses to both genders might fail to represent real-world ergonomic constraints, leading to optimized postures that diverge from empirical behavior.

Analysis of the weighted scores indicates that the influence of EWF on RWF is stronger than the influence of RWF on EWF. One contributing factor is the predefined benchmark posture. When one posture holds favorable ergonomic performance, the reachability performance is largely reduced. Conversely, ergonomic performance shows comparatively less deterioration when reachability requirements are satisfied. The benchmark posture was adopted from existing literature, yet it might not be fully representative of the SUV or sedan vehicle architecture in this study. More realistic ergonomic postures derived from measurements in actual vehicles should be taken into account.

A new packaging design with revised seat and steering wheel adjustment areas is proposed based on the distribution of drivers' CPs and HPs obtained from optimized postures. Drivers' postures are re-optimized within this new packaging. The reachability performance of all drivers and the ergonomic performance of several drivers show improvement. Through iterative cycles of packaging design proposals and posture optimization, a packaging that accommodates all drivers might be achievable within the design space. However, the feasibility of these proposed designs has not been validated within an actual vehicle architecture model.

This study has several limitations. The distributions of optimized CPs are not compared with empirical distributions due to the lack of available data. In addtion, although potential factors underlying the different influence of RWF and EWF on each other are discussed, they are not validated. Despite that driving comfort is also affected by factors such as the thermal environment of the vehicle, driver fatigue, actions, and driving duration [4, 17, 16], this study considers only the biomechanical aspects of driver posture. Finally, it might be unrealistic for each reachable or ergonomic response to share the same weight in respective category using RWF or EWF. Certain responses such as visibility should function as hard constraints that must not be violated, while constraints related to head, knee, or leg freedom may tolerate some violation.

5 CONCLUSIONS AND OUTLOOK

Seven digital drivers are modeled using AD, and their postures are optimized within the packaging design in CATIA. RWF and EWF are introduced to investigate postures under differently prioritized reachable and ergonomic responses. The results indicate that the optimized postures represent a trade-off between reachable and ergonomic constraints, and that simultaneously improving reachability and ergonomics for all drivers is challenging. Based on the optimized postures, new packaging designs are proposed to enhance the reachable and ergonomic performance of all digital drivers. The universality of this method is demonstrated by adapting the SUV architecture model to a sedan.

Compared with previous methods based on the SAE template, this method enables dynamic interaction between digital drivers and vehicle packaging geometries. Posture performance is intuitively visualized and analyzed using quantitative scores, supporting real-time evaluation. The iteratively developed new packaging designs illustrate possible design directions tailored to realistic use cases. Overall, this method provides an efficient and cost-effective solution for improving vehicle packaging design.

In future work, differences in female HPs will be examined using additional female models and expanded geometric constraints. Both reachable and ergonomic responses will be individually weighted, and ergonomic responses will be formulated in a more gender-specific manner to better accommodate male and female drivers. Benchmark postures will be self measured to accommodate the vehicle architecture models. Furthermore, the optimized postures will be validated in real vehicles or mock-ups to assess the practical applicability of the proposed approach.

ACKNOWLEDGEMENTS

This research has been supported by BMW Nachwuchsprogramme and the BMW Research and Innovation Center.

ORCID

Runze Li, http://orcid.org/0009-0009-7073-9680
Lukas Berk, http://orcid.org/0000-0002-4629-2286

REFERENCES

[1] Barbieri, L.; Muzzupappa, M.: Performance-driven engineering design approaches based on generative design and topology optimization tools: A comparative study. Applied Sciences, 12(4), 2022. ISSN 2076-3417. http://doi.org/10.3390/app12042106.

[2] Bhise, V.D.: Ergonomics in the Automotive Design Process. CRC Press, 2008. ISBN 9781420064546.

[3] Gen, M.: Genetic algorithms and their applications. In Springer Handbook of Engineering Statistics, 749–773. Springer London, London, 2006.

[4] George, M.S.; Neil, J.M.; Mike, F.: Improving long term driving comfort by taking breaks – how break activity affects effectiveness. Applied Ergonomics, 65, 81–89, 2017. ISSN 0003-6870. http://doi.org/https://doi.org/10.1016/j.apergo.2017.05.008.

[5] Gräßler, I.; Preuß, D.; Brandt, L.; Mohr, M.: Efficient formalisation of technical requirements for generative engineering. Proceedings of the Design Society, 3, 1595–1604, 2023. http://doi.org/10.1017/pds.2023.160.

[6] Grünen, R.E.; Günzkofer, F.; Bubb, H.: Anatomical and Anthropometric Characteristics of the Driver, 161–217. Springer Fachmedien Wiesbaden, Wiesbaden, 2021. ISBN 978-3-658-33941-8. http://doi.org/10.1007/978-3-658-33941-8_4.

[7] Haroon, S.M.; Panhorst, J.D.; Ryan, A.; Nasrin, S.: Comparing steering wheel proximity: Differences in seating distance between male and female drivers. Journal of Transport & Health, 44, 102111, 2025. ISSN 2214-1405. http://doi.org/https://doi.org/10.1016/j.jth.2025.102111.

[8] Human Accom and Design Devices Stds Comm: Devices for use in defining and measuring vehicle seating accommodation. Tech. rep., SAE International, 400 Commonwealth Drive, Warrendale, PA, United States, 2021.

[9] Inês, C.; Luís, S.; António, L.: Computational design in architecture: Defining parametric, generative, and algorithmic design. Frontiers of Architectural Research, 9(2), 287–300, 2020. ISSN 2095-2635. http://doi.org/https://doi.org/10.1016/j.foar.2019.12.008.

[10] Jung, M.; Cho, H.; Roh, T.; Lee, K.: Integrated framework for vehicle interior design using digital human model. Journal of Computer Science and Technology, 24, 1149–1161, 2009. http://doi.org/10.1007/s11390-009-9287-3.

[11] Junk, S.; Rothe, N.: Lightweight design of automotive components using generative design with fiber-reinforced additive manufacturing. Procedia CIRP, 109, 119–124, 2022. ISSN 2212-8271. http://doi.org/https://doi.org/10.1016/j.procir.2022.05.224. 32nd CIRP Design Conference (CIRP Design 2022) - Design in a changing world.

[12] König, A.; Schockenhoff, F.; Koch, A.; Lienkamp, M.: Concept design optimization of autonomous and electric vehicles. In 2019 8th International Conference on Power Science and Engineering (ICPSE), 44–49, 2019. http://doi.org/10.1109/ICPSE49633.2019.9041175.

[13] König, A.; Telschow, D.; Nicoletti, L.; Lienkamp, M.: Package planning of autonomous vehicle concepts. Proceedings of the Design Society, 1, 2369–2378, 2021. http://doi.org/10.1017/pds.2021.498.

[14] Leitão, A.; Garcia, S.: Reverse algorithmic design. In J.S. Gero, ed., Design Computing and Cognition'20, 317–328. Springer International Publishing, Cham, 2022. ISBN 978-3-030-90625-2.

[15] Manary, M.A.; Reed, M.P.; Flannagan, C.A.C.; Schneider, L.W.: Atd positioning based on driver posture and position. SAE Transactions, 107, 2911–2923, 1998. ISSN 0096736X, 25771531. http://www.jstor.org/stable/44741245.

[16] Mika, S.; Shin-ichi, S.; Aryel, B.; Khai, J.K.; Mototaka, Y.: Analysis of the effect of thermal comfort on driver drowsiness progress with predicted mean vote: An experiment using real highway driving conditions. Transportation Research Part F: Traffic Psychology and Behaviour, 94, 517–527, 2023. ISSN 1369-8478. http://doi.org/https://doi.org/10.1016/j.trf.2023.03.009.

[17] Park, S.J.; Kim, S.W.; Kim, C.J.; Kwon, K.S.: A study on the assessment of driver's fatigue. SAE Transactions, 111, 1168–1172, 2002. ISSN 0096736X, 25771531. http://doi.org/https://doi.org/10.4271/2002-01-0784.

[18] Parkinson, M.; Reed, M.: Optimizing vehicle occupant packaging. SAE Technical Papers, 2006. http://doi.org/10.4271/2006-01-0961.

[19] Reed, M.; Manary, M.; Flannagan, C.; Schneider, L.: Effects of vehicle interior geometry and anthropometric variables on automobile driving posture. Human Factors, 42, 541–552, 2000. http://doi.org/10.1518/001872000779698006.

[20] Reed, M.; Manary, M.; Flannagan, C.; Schneider, L.: A statistical method for predicting automobile driving posture. Human factors, 44, 557–68, 2002. http://doi.org/10.1518/0018720024496917.

[21] Reed, M.; Roe, R.; Manary, M.; Flannagan, C.; Schneider, L.: New concepts in vehicle interior design using aspect. SAE Technical Papers, 1999. http://doi.org/10.4271/1999-01-0967.

[22] Reed, M.; Roe, R.; Schneider, L.: Design and development of the aspect manikin. SAE Technical Papers, 1999. http://doi.org/10.4271/1999-01-0963.

[23] Reynolds, M.; Scataglini, S.: Driver comfort and gender inequality measured with DHMs. In Digital Human Modeling and Applied Optimization. AHFE International, 2022.

[24] Schockenhoff, F.; König, A.; Koch, A.; Lienkamp, M.: Customer-relevant properties of autonomous vehicle concepts. Procedia CIRP, 91, 55–60, 2020. http://doi.org/10.1016/j.procir.2020.02.150.

[25] Schockenhoff, F.; König, A.; Zähringer, M.; Lienkamp, M.: User need-oriented concept development of autonomous vehicles. Proceedings of the Design Society, 1, 3349–3358, 2021. http://doi.org/10.1017/pds.2021.596.

[26] Upmann, A.: Application of Digital Human Modeling for the Ergonomic Evaluation of Handbrakes in Passenger Vehicles. Deutsche Sporthochschule Köln, 2016.

[27] van der Meulen, P.; Seidl, A.: Ramsis – the leading cad tool for ergonomic analysis of vehicles. In V.G. Duffy, ed., Digital Human Modeling, 1008–1017. Springer Berlin Heidelberg, Berlin, Heidelberg, 2007. http://doi.org/https://doi.org/10.1007/978-3-540-73321-8_113.

[28] Wang, Q.; Shang, Y.; Qin, Z.; Xu, H.; Jiang, W.; Li, H.; Zhang, G.: Comfort evaluation and position parameter optimization of the steering wheel in agricultural machinery based on a three-level evaluation index system. International Journal of Agricultural and Biological Engineering, 15, 214–222, 2022. http://doi.org/10.25165/j.ijabe.20221504.6318.

[29] Yoo, S.; Lee, S.; Kim, S.; Hwang, K.H.; Park, J.; Kang, N.: Integrating deep learning into cad/cae system: generative design and evaluation of 3d conceptual wheel. Structural and Multidisciplinary Optimization, 64, 2021. http://doi.org/10.1007/s00158-021-02953-9.

[30] Zhao, N.; Parthasarathy, M.; Patil, S.; Coates, D.; Myers, K.; Zhu, H.; Li, W.: Direct additive manufacturing of metal parts for automotive applications. Journal of Manufacturing Systems, 68, 368–375, 2023. ISSN 0278-6125. http://doi.org/https://doi.org/10.1016/j.jmsy.2023.04.008.